Simulation of Planar Welding Flows: Part 2. Strain History, Stress Calculation, and Experimental Comparison

K. H. WEI, M. E. NORDBERG III, *and* H. H. WINTER

Department of Chemical Engineering
Goessmann Laboratory
University of Massachusetts
Amherst, Massachusetts 01003

A numerical method is described for calculating the stress a viscoelastic melt exhibits in a flow, based on approximate kinematics. The method assumes that the kinematics are reasonably close to those of a shear-thinning fluid such as the Carreau model. The strain history of a given flow and the resulting stress are calculated via a tracking method from finite element kinematics. Full-field flow birefringence experiments were done for low-density polyethylene and polystyrene flowing past a thin plate divider in a 1.254-mm planar slit die. By digitally analyzing birefringence photographs of the flow field, the birefringence was measured over two dimensions. These birefringence results are in good agreement with birefringence fields calculated from the numerical simulations and the stress-optical law. The flow fields were most highly oriented in a region surrounding the weld interface just downstream of the plate divider. This orientation relaxed farther downstream, with polystyrene relaxing faster than low-density polyethylene.

INTRODUCTION

Welding flows occur in polymer processing when two streams of molten polymer meet to form a weld interface. The result is often referred to as a "weld line" since the weld interfaces appear as lines on the surface of polymeric parts. The macromolecules near the interface are highly oriented because of their deformation history of large strains (1). This orientation of macromolecules and the lack of tie molecules across the interface reduce the mechanical properties in the transverse direction; it is not yet known whether molecule orientation enhances or reduces the diffusion process across the weld interface. Enhancement of the diffusion would be advantageous for improving the mechanical properties after solidification. In this study, we are interested in determining the molecular orientation near the weld interface without discussing its effect on the diffusion or on mechanical properties.

The anisotropy of birefringence is a measure of molecular orientation. Molecular orientation therefore can be calculated indirectly with the stress-optical law, which states that the (deviatoric) refractive index and stress ellipsoids are coaxial and similar; i.e., the principal values of birefringence and stress are proportional (2). Flow-induced molecular orientation in a material therefore can be modeled by the stress tensor components calculated as a function of its strain history.

Calculated values of molecular orientation can be compared with experimental values measured by the rheo-optical method. This method gives extensive information concerning the stress in the flowing polymer without distorting the flow field (3–6). In this study, we use the rheo-optical method for measuring the birefringence of polymer melts in flow past an obstacle. Molecular orientation was generated by plane flows past a plate divider in a slit. The main objective is to understand the effect of viscoelasticity on the stress in flow past obstacles.

STRESS

Memory Function

For polymer melts, many different constitutive equations have been derived from continuum mechanics or from molecular models (7, 8). For this study, we selected a memory integral equation that is based on the rubberlike liquid (9):

$$\tau(t) = \int_{-\infty}^{t} m(t, t')C^{-1}(t, t')dt' \quad (1)$$

where τ is a stress tensor, m is a memory function, and C^{-1} is the Finger strain tensor. The memory function can be separated into time-dependent part and strain-dependent part (10):

$$m(t, t') = \dot{m}(t, t')h(I_1, I_2) \quad (2)$$

with

$$\dot{m}(t,t') = \sum_{i=1}^{n} \frac{g_i}{\lambda_i} \exp\left(\frac{-(t - t')}{\lambda_i}\right) \quad (3)$$

$$h(I_1, I_2) = f \exp(-n_1 \sqrt{I}) + (1 - f) \exp(-n_2\sqrt{I}) \quad (4)$$

$$I = \alpha I_1 + (1 - \alpha)I_2 \quad (5)$$

where $\dot{m}$ is the memory function for linear viscoelastic data, h is a strain functional, g_i are nonnegative coefficients, λ_i are relaxation times, and f, n_1, n_2, α are chosen empirically to fit nonlinear experiments (11). This equation has been extensively tested in several rheological experiments. It describes the rheological behavior of polymer melts in most transient shear flows (12). However, it is only marginally adequate for describing extensional flows (13).

Strain History

Stress and kinematics in a continuum are coupled in a system of equations consisting of constitutive equations, conservation of mass and of linear momentum, and the boundary conditions. A complete solution of the coupled system of equations, including a realistic rheological constitutive equation (such as a memory integral equation with a spectrum of relaxation times), is not possible with the current state of the art (14). However, it is important to determine the stress from the rheological behavior as observed in the laboratory, and we will attempt this by an approximate method (15). In this approximate method, the calculated kinematics from inelastic models are used as approximate solutions for real flows and for determining strain histories. We are then able to calculate the stress developed in a polymeric material element as if it had been subjected to this prescribed deformation (approximate kinematics). The calculated stress will resemble the actual stress in the flowing polymer provided that both the approximate and the real kinematics have common basic features (no additional vortex, for example). The sensitivity of the stress to small quantitative deviations in the kinematics will be used as a criterion for the range of applicability of the approximate method.

PRESCRIBED KINEMATICS

In many flows, the kinematics of an inelastic fluid are very close to those of polymer melts (16). Therefore, as an approximation, the kinematics of inelastic liquids (Newtonian and Carreau) are used in this study. The kinematics of ideal welding flows generated by a thin plate divider in a slit channel were obtained by using a finite element analysis in the first part of this study (17). The assumptions were that the flow is steady, isothermal, and two-dimensional. That work concluded that extensional flow dominates the region downstream from the stagnation point of the plate divider, and that the fluid elements near the weld interface have a strain history of both high stretching and shearing. In the following, we will consider only one case, a typical welding flow, with the dividing and merging of a fluid stream. The flow, the shape, and the location of the plate divider for the case are assumed to be symmetric, as shown in *Fig. 1*. For the above approximation, the next step is to calculate the strain history of material elements.

TRACKING

Many different techniques have been proposed for calculating the strain history of a material element in a given flow (tracking). Viriyayuthakorn and Caswell (18) determined the strain history from the displacement of the nodes of a convected finite element. Their scheme is limited to small strains. Bernstein, *et al.* (19) used a quadrilateral element with a uniform velocity gradient within triangles. Their procedure is not immediately applicable to arbitrary types of elements. Winter (15) derived the tracking equations for steady axisymmetric flow and demonstrated their validity. He showed that the tracking equations are in the most simple form when written in terms of a Lagrangian coordinate system that translates and rotates with the flow (see *Fig. 2*). Dupont, *et al.* (20) derived the same tracking equations in different notation and applied them to a finite element program for memory fluids. Adachi (21) rederived the tracking equations via a third method and found agreement with the earlier results of Winter and Dupont, *et al.* In this paper, we use Winter's scheme and Nordberg's program (22) to compute the strain history of material elements along their path lines.

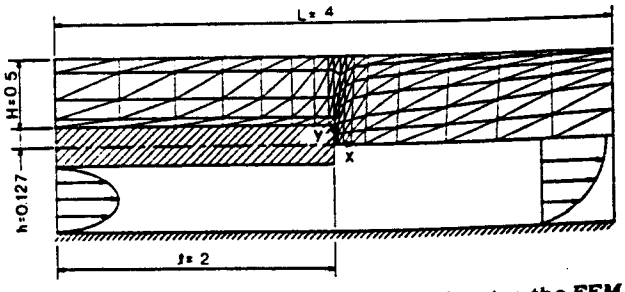

Fig. 1. Schematic of the flow geometry showing the FEM mesh used to obtain approximate kinematics and typical inlet and outlet velocity profiles.

The basic equations of the tracking procedure are given in the following in terms of planar coordinates. The more general axisymmetric case is given by Winter (15). The starting point of this tracking procedure is a given velocity field, $v(x, y)$, of a steady planar flow. The first step in the calculation is the determination of the streamline, $y(x)$, of a material element of given stream function value ψ:

$$\psi = \frac{\int_{y_i}^{y(x)} \rho v_x dy}{\int_{y_i}^{y_o} \rho v_x dy} = \text{constant} \qquad (6)$$

where y_i and y_o are the inner and the outer bounds of the flow and ρ is the density of the polymer. The second step is the determination of the elapsed time $t - t'$ that a material element needs to travel from position x' to x:

$$t - t' = \int_{x'}^{x} \frac{dx}{v_x}\bigg|_{\psi=\psi^*}. \qquad (7)$$

The integration has to be taken along the streamline ψ = constant. This time difference will be needed when combining strain and relaxation modulus in the constitutive equation. The kinematic variables now can be expressed in terms of time:

$$v(x') = v(t') = v', \qquad (8)$$

$$y(x') = y(t') = y'. \qquad (9)$$

The third step is the calculation of the shear angle for the deformation relative to the point where the stress is desired as a function of time.

$$\gamma' = -\rho' v'^2 \int_{t'}^{t} \frac{\dot{\gamma}''_{tn}}{\rho'' v''^2} dt'', \qquad (10)$$

where v is the magnitude of the velocity vector

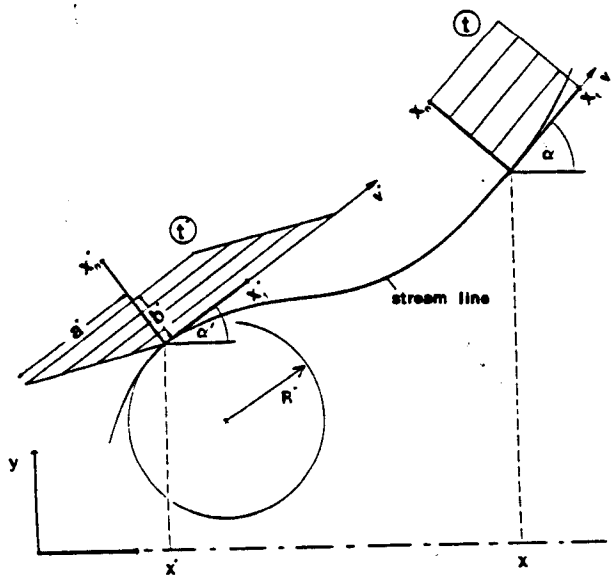

Fig. 2. Deformation of a material element in a tangent-normal ($x_t - x_n$) coordinate system.

v. The shear rate $\dot{\gamma}_{tn}$ in a streamline coordinate system (x_n, x_t) as shown in *Fig. 2* is defined as

$$\dot{\gamma}_{tn} = \dot{\gamma} : x_n x_t. \qquad (11)$$

The detailed derivation of this equation is given in the *Appendix*.

With this information, we can determine the components of the Finger strain tensor, which describes the strain of a material element that travels along the streamline ψ = constant from the position x' to the position x.

$$C^{-1}(t, t') = \mathcal{Q} \cdot \begin{bmatrix} (1 + \gamma'^2)\left(\frac{v}{v'}\right)^2 & -\gamma' \frac{\rho'}{\rho} & 0 \\ -\gamma' \frac{\rho'}{\rho} & \left(\frac{\rho' v'}{\rho v}\right)^2 & 0 \\ 0 & 0 & 1 \end{bmatrix} \cdot \mathcal{Q}^T \qquad (12)$$

The reference state of the strain tensor is chosen at time t or position x. The rotation matrix

$$\mathcal{Q} = \begin{bmatrix} \cos\alpha & \sin\alpha & 0 \\ -\sin\alpha & \cos\alpha & 0 \\ 0 & 0 & 1 \end{bmatrix} \qquad (13)$$

depends on the slope of the streamline (angle α) at position x.

Inspecting the above series of equations, one sees that all that is needed to calculate the strain is the time-dependent position of a streamline, and values of density, velocity, shear rate, and flow direction along the streamline. The above equations form the basis for a stress calculation method. Specifically, we apply them now to calculate the strain history and stress for a material element traveling through a finite element grid.

NUMERICAL PROCEDURE

The tracking procedure gives the positions of the path lines and the velocity gradients of individual material elements. Analytical procedures to construct path lines on a finite element grid have been proposed (18, 20). A simple numerical procedure to construct the streamlines by converting kinematics calculated from the finite element method (FEM) is presented here. The procedure can be described as follows:

The first step is to choose a set of grid lines perpendicular to the main flow direction (i.e., lines of constant x, see *Fig. 3*). Next, *Eq 1* is integrated numerically for the stream function in a stepwise fashion along each grid line to find (with additional interpolation) the transverse positions of a given set of streamlines, $\psi = \psi_i^*$. The streamlines thus constructed are divided into small intervals by the grid lines. For each interval, the contribution to the deformation is calculated from *Eqs 10* and *12*. Each time a velocity or velocity gradient component is

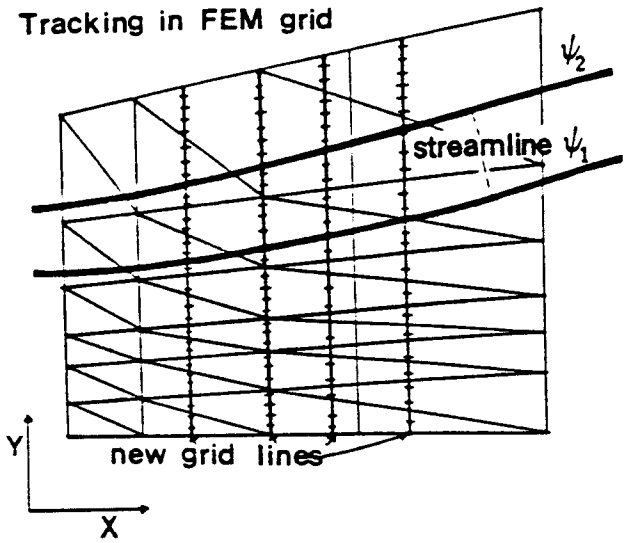

Fig. 3. New grid lines superimposed on the FEM mesh for the location of a set of streamlines and later tracking along these streamlines.

needed at a given point in both the integration and the actual tracking, it is calculated by directly evaluating the FEM shape function for the triangle where the point is located.

The total stress is then calculated by integrating all intervals going backward toward the inlet. The stress calculation is terminated when the contribution from the last interval to the total normal stress is substantially small. If the inlet of the flow is reached, the calculation is continued by extending the inlet region fictitiously, based on the assumption that the flow is fully developed upstream of the inlet.

FLOW BIREFRINGENCE MEASUREMENTS IN THE 1-2 PLANE

An experiment was set up to measure the birefringence in welding flows of polymer melts. This setup includes a Göttfert rheometer, a slit die, and optical components. The Göttfert rheometer consists of a polymer reservoir and a hydraulic piston that forces the polymer from the reservoir into the die. The slit die was constructed specifically for carrying out flow birefringence measurements. It consists of a rectangular slit with two glass windows, one on each smaller side of the slit. The flow is split at the entrance to the die by a plate divider, and then the two streams recombine at about the center of the die. The dimensions of the slit die are shown in *Fig. 4*. The aspect ratio of the slit is 10:1, resulting in an approximately two-dimensional flow geometry.

The optical system consists of a light source, a green filter, a condenser, a polarizer, and two quarter-wave plates. The schematics of this setup are shown in *Fig. 5*.

The flow birefringence measurements are briefly described here. A polarized monochromatic green light passes a quarter-wave plate then travels along the 3-direction through the

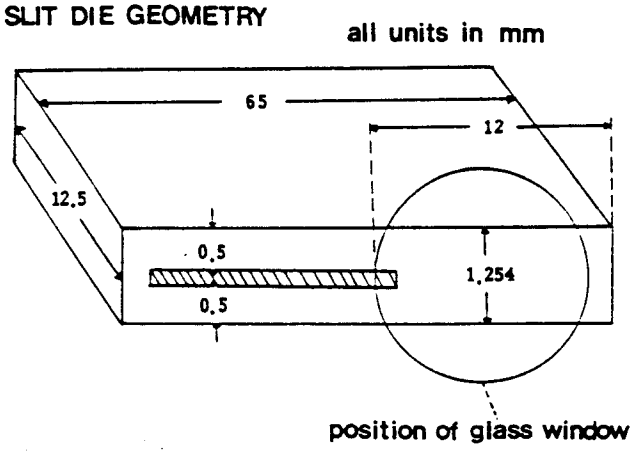

Fig. 4. Dimensions of the slit die used in the flow birefringence experiments.

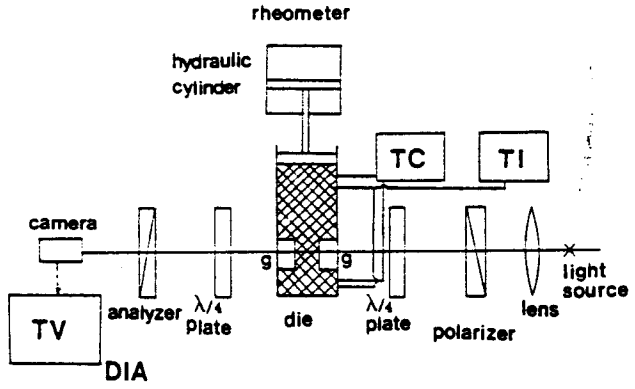

Fig. 5. Schematic diagram of the optical equipment used for flow birefringence measurements.

die. (The 1-direction is the natural flow direction, the 2-direction is the perpendicular in the plane of flow, and the 3-direction is normal to this plane.) The light emerging from the slit die passes through the second quarter-wave plate and an analyzer, finally reaching a camera. The volume flow rate of the tested polymer melt was precisely controlled by a microprocessor in the Göttfert rheometer. A pressure transducer flush-mounted near the entrance of the slit measures the total pressure drop through the die. There are five independent temperature controllers along the barrel and the slit die (three surrounding the slit die). There are also three temperature indicators along the slit die. By adjusting these devices, the temperature at different positions could be controlled to isothermal conditions within 1 K.

Values of the stress-optical coefficient for polystyrene and low-density polyethylene (*Table 1*) were taken from Wales's work (23). The birefringence in the 1-2 plane of a steady, isothermal flow in a slit is measured by using a circular polariscope. The equations for the circular polariscope and for the birefringence in terms of phase angle are given by

$$I = I_0 \sin^2\left(\frac{\delta}{2}\right) \qquad (14)$$

Table 1A. The Material Data of the Polymers Studied.

Polymer	λ_i(s)	Discrete Relaxation Spectrum g_i (Pa)
LDPE	5.913×10^{1}	3.776×10^{1}
T = 150°C	1.817×10^{1}	3.710×10^{2}
	3.680×10^{0}	1.952×10^{3}
	6.606×10^{-1}	1.085×10^{4}
	1.073×10^{-1}	2.806×10^{4}
	2.060×10^{-2}	6.040×10^{4}
	3.026×10^{-3}	1.371×10^{5}
	3.381×10^{-4}	3.027×10^{5}
PS	5.152×10^{1}	7.763×10^{1}
T = 180°C	8.669×10^{0}	1.338×10^{3}
	5.135×10^{0}	9.275×10^{2}
	1.018×10^{0}	1.762×10^{4}
	1.107×10^{-1}	5.004×10^{4}
	1.065×10^{-2}	6.978×10^{4}
	9.927×10^{-4}	1.009×10^{5}
	5.821×10^{-5}	5.558×10^{5}

The Parameters for Temperature-dependent Shift Factors

Activation Polymer	Temperature (°C)	C_1	C_2	(K)	Energy (kcal/mole)
LDPE	150				12,600
PS	180	5.61	143.2		—

Table 1B. Parameters for the Approximation of Measured Shear Strain Function.

Approximation Function	Parameters	LDPE (150°C)	PS (180°C)
$h(\gamma) = f\exp(-n_1\gamma)$	f	0.67	0.88
$+ (1-f)\exp(-n_2\gamma)$	n_1	0.304	0.377
	n_2	0.070	0.073

Table 1C. Rheological Parameters of Polymers Used in the Simulations.

	Polymers	
	LDPE	PS
Reference temperature, T_0 (°C)	150	180
Carreau model parameters		
Infinite-shear-rate viscosity, η_∞ (Pa.s)	0	0
Zero-shear-rate viscosity, η_0 (Pa.s)	2.81×10^{4}	4.47×10^{4}
Time constant, λ (s)	2.09	2.06
Stress-optical coefficient,* C (Pa^{-1})	2.1×10^{-9}	-4.1×10^{-9}

*Values obtained from Wales (23).

$$\Delta n = \frac{\lambda\delta}{2\pi d}. \qquad (15)$$

In the above equations δ is the phase angle of the polarized light, I is the intensity of the emerging light, I_0 is the intensity of the incident light, Δn is the birefringence, λ is the wavelength of the monochromatic light, and d is the thickness of the slit. *Equation 14* relates the intensity of the incident beam to that of the emerging beam of circularly polarized light. *Equation 15* defines the relation between phase angle and birefringence. If a monochromatic light source is used, the birefringence value where dark bands appear is described by *Eq 16*.

$$\Delta n = \frac{k\lambda}{d} \qquad (16)$$

where k is an integer number and is called the order of the dark bands.

At the start of an experiment, the flow device was heated to the desired temperature, and the polymer was put into the barrel. The extrusion started at a very low speed (0.01 mm/s) after the polymer was completely melted and equilibrated for 20 min. The polymer was then extruded at the desired speed. Pictures were taken only after the birefringence was fully developed and the pressure reading became stable. First, white light was used to get a whole-field birefringence picture. From the color bands of the picture, isotropic lines or points (no molecular orientation difference, $\Delta n = 0$) were identified and located. The isotropic regions appeared as dark bands (or points) since the background of the light measurement was set to be dark. A second picture was taken with a monochromatic light source (green light) to get green and dark bands. By comparing the two pictures, the order of dark bands could be determined. From the order of the dark band and by using *Eq 16*, the birefringence value at each dark band could be calculated. In most cases, the dark bands alone provided enough data points.

To obtain light intensity values at different positions, the intensity of the emerging beam recorded on film was evaluated through a digital image analysis technique (University of Massachusetts Computing Center, Digital Image Analysis Laboratory). Different cross sections of the slit were chosen for analysis. Lines along different cross sections were drawn and light intensity values along these lines were plotted (see *Fig. 6*). For comparison, the birefringence was also calculated from stress model:

$$\Delta n = C[(\tau_{11} - \tau_{22})^2 + 4\tau_{12}^2]^{1/2} \qquad (17)$$

where Δn is the difference in refractive indices, $\tau_{11} - \tau_{22}$ is the first normal stress difference, τ_{12} is the shear stress, and C is a stress-optical coefficient.

The linearity of the stress-optical law has been discussed in detail by Janeschitz-Kriegl (2): In shear flows the stress-optical law holds up to shear rates of about 10 s^{-1} and in extensional flow up to extension rates of 0.065 s^{-1} for a variety of polymer melts.

MEASURED BIREFRINGENCE AND COMPARISON WITH SIMULATION

Birefringence Distribution for LDPE in the Slit

For low-density polyethylene (LDPE) processed at 160°C with an average outlet velocity of 0.8 mm/s, the birefringence pattern observed with monochromatic light is presented in *Fig. 7*. This photograph was analyzed as described above to obtain birefringence values at different cross sections (different x values) of the slit. The resulting profiles are shown in *Fig. 8*, suc-

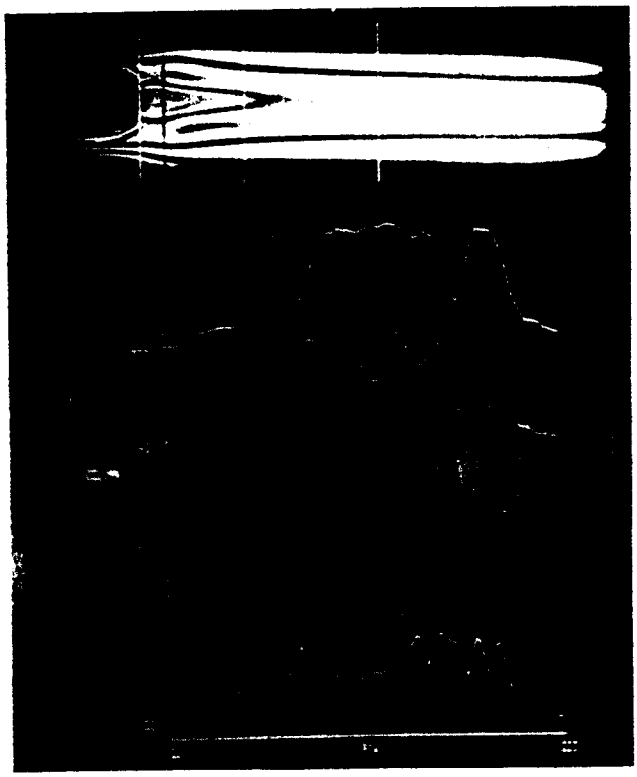

Fig. 6. Typical digital image analysis output. The raw birefringence photograph is crossed by several lines. Light intensity vs. transverse position is plotted for each of these lines.

Fig. 7. Birefringence pattern for LDPE at 160°C with an average outlet velocity of 0.8 mm/s.

cessively shifted by 10^{-4} for clarity. Near the stagnation point, $x = 0$ and $y = 0$, the birefringence reaches a maximum, which is due to the intense elongational flow behavior (stretching). Away from the weld interface, toward the wall, the birefringence value starts decreasing, which is caused by reduced elongational flow. Further toward the wall, a minimum occurs because material elements along path lines at this point have experienced either little stretching or little shearing along their path lines. Near the wall, the birefringence value increases very quickly, which results from the intense shear flow close to the wall. The order of magnitude of the birefringence near the wall and near the stagnation point is about the same at a cross section near the stagnation point. At a cross section just downstream of the stagnation point, molecules are highly oriented in the flow direction. Farther downstream of the plate divider, the birefringence peak near the weld interface starts decreasing gradually. However,

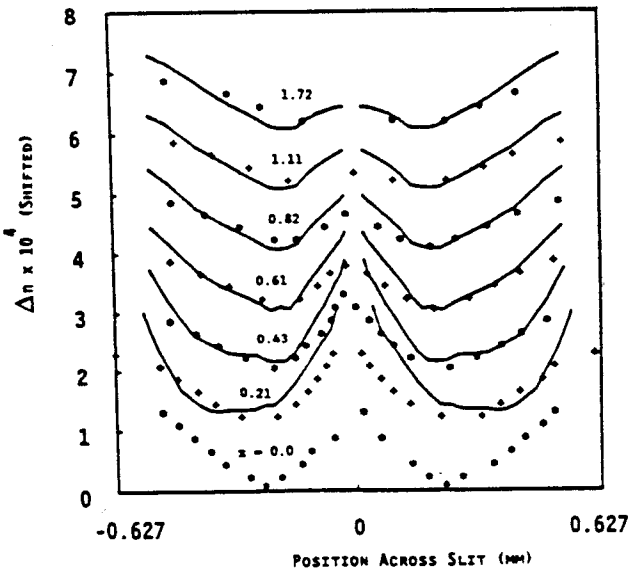

Fig. 8. Comparison of experimental results (points) and simulation results (lines) for LDPE at 160°C and 0.8 mm/s average velocity. In this figure and in subsequent ones the birefringence values are successively shifted up by 1×10^{-4} for clarity.

the molecular orientation difference near the weld interface is still retained to some extent. In fact, LDPE does not relax to an isotropic state as it would in a shear flow on the centerline even two flow channel widths downstream of the stagnation point.

The calculated birefringence is also plotted in *Fig. 8*. The calculated birefringence is based on kinematics from the Carreau model with rheological parameters of the polymer taken from the literature (24). They agree with each other fairly well in the region near the two minimums. However, disagreement happens near the centerline and near the walls. This can be caused by several factors. In the region close to walls and near the stagnation point, measurements became difficult since the resolution of the picture is limited by the resolution of optical equipment and alignment of devices. The finer the fringes are, the shorter are the distances between maximum intensities and minimum intensities. If the distances between the maximum and the minimum intensities are shorter than the inverse of the resolution of the optical equipment such as lenses of the camera, these intensities can not be registered distinctly. Rather, averaged intensities were registered. Additionally, the fact that optical devices are slightly out of alignment can make fringes less discernible.

Figures 9 and *10* show, in like manner, the raw birefringence pattern and digital image analysis results for LPDE with the volume flow rate doubled with respect to *Figs. 7* and *8*. The molecular orientation difference increases mildly with respect to the first case and the region that has orientation differences broadens. In a distance of two flow channel widths

Fig. 9. Birefringence pattern for LDPE at 160°C with an average outlet velocity of 1.6 mm/s.

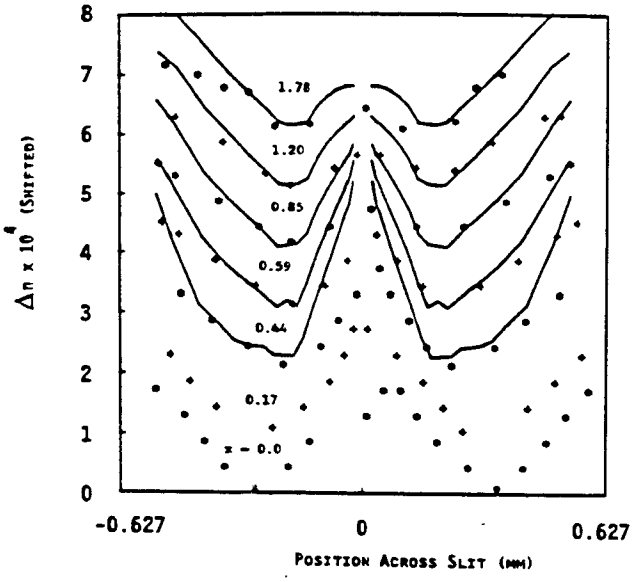

Fig. 10. Comparison of experimental results (points) and simulation results (lines) for LDPE at 160°C and 1.6 mm/s average velocity.

Fig. 11. Birefringence pattern for PS at 180°C with an average outlet velocity of 0.1 mm/s.

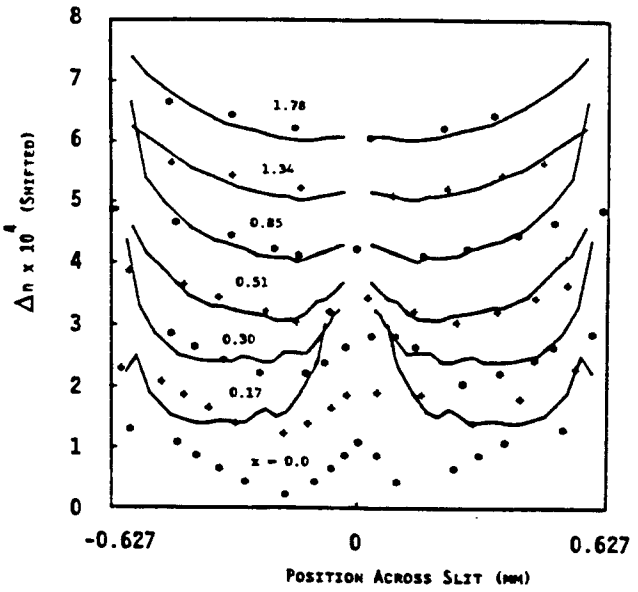

Fig. 12. Comparison of experimental results (points) and simulation results (lines) for PS at 180°C and 0.1 mm/s.

downstream of the stagnation point, the birefringence peak still exists.

Birefringence Distribution for PS in the Slit

In *Fig. 12*, the birefringence for polystyrene (PS) processed at 180°C with an average exit velocity of 0.1 mm/s is plotted at different cross sections along the slit. The corresponding photograph is *Fig. 11*. The birefringence pattern across the slit displays two minimums and one maximum that are similar to those of LDPE but with several subtle differences. First, the oriented region near the centerline is narrower and the orientation difference near the weld interface is smaller than they were for LDPE. This is basically due to different processing conditions and different molecular parameters (polarizability, refractive index). A second difference is that the relaxation of the oriented layer depends strongly on the molecular structure. The linear PS relaxes very quickly. Within a distance of one-and-a-half flow channel widths away from the stagnation point, the birefringence reduces approximately to that exhibited in a simple shear flow. The long-chain-branching LDPE requires a long distance to "forget" the influence of prehistory and to develop the stress fully. This is consistent with the study of birefringence in the 1-3 plane in slits done by Wales (23).

CONCLUSION

Model

The model, which is based on approximate kinematics and continuum mechanics, gives good predictions of molecular orientation differences in a two-dimensional welding flow despite the fact that the rheological characterization was performed in very ideal experiments (step shear). The agreement between simulations and experiments is excellent in cases of low polymer flow rates. The model is insensitive to small deviations in kinematics such as those resulting from a change of power-law index.

Experiments

The combination of the flow birefringence technique and the digital image analysis can provide a measurement of molecular orientation at any point of a two-dimensional flow field. The macromolecules near the starting point of the weld interface are highly oriented in the main flow direction. When the flow rate of polymers increases, the size of the oriented region and its orientation difference increases. The macromolecular orientation relaxes slowly in the long-chain-branching LDPE and relaxes quickly in the linear PS.

APPENDIX

The objective of the derivation is to find the strain of a material element in a continuum which moves with *known* velocity $v(x, y)$. This method is briefly described here. First, we consider the steady motion of a fluid. The Finger strain tensor, $C^{-1}(t, t')$, is a measure of the large deformation of a material element from a time t' to a later time t. It is the inverse of the Cauchy-Green strain tensor, which is defined in terms of the deformation gradient:

$$C(t, t') = F(t, t')^T \cdot F(t, t') \tag{A1}$$

The deformation gradient tensor, $F(t, t')$, in turn, relates the state of a given infinitesimal vector (dx) to its state at some previous time (dx') along the path line traced by the material point.

$$dx' = F \cdot dx \tag{A2}$$

If relations between corresponding three pairs of vectors (dx_1, dx_2, dx_3) and (dx_1', dx_2', dx_3') are known, F can be determined readily. Following the notation of Winter (15), we consider the past vector $d\bar{x}'$ as it travels the path line. The scalar components of $d\bar{x}'$ in a local tangent-normal ($t - n$) coordinate system can be defined as follows (*Fig. 2*):

$$\begin{aligned} d\bar{x}_1' &= (u', 0, 0); & d\bar{x}_1 &= (u, 0, 0) \\ d\bar{x}_2' &= (a', b', 0); & d\bar{x}_2 &= (a, b, 0) \\ d\bar{x}_3' &= (0, 0, 1); & d\bar{x}_3 &= (0, 0, 1) \end{aligned} \tag{A3}$$

$$\gamma' = \frac{a'}{b'}; \qquad \gamma = \frac{a}{b} \tag{A4}$$

where $b = \dfrac{1}{\rho v}$, and γ' is the tangent of the shear angle for the material vector.

To compare results with experiments, these vectors need to be rotated by angles between local coordinate systems and global coordinate system. From *Eq A3*, three independent material vectors at both times uniquely determine all nine components of F in the global coordinate system:

$$\begin{aligned} \mathcal{Q}' \cdot d\bar{x}_1' &= F \cdot (\mathcal{Q} \cdot d\bar{x}_1) \\ \mathcal{Q}' \cdot d\bar{x}_2' &= F \cdot (\mathcal{Q} \cdot d\bar{x}_2) \\ \mathcal{Q}' \cdot d\bar{x}_3' &= F \cdot (\mathcal{Q} \cdot d\bar{x}_3) \end{aligned} \tag{A5}$$

In more concise notation:

$$\mathcal{Q}' \cdot \bar{X}' = F \cdot (\mathcal{Q} \cdot \bar{X}) \tag{A6}$$

where $\bar{X}' = (d\bar{x}_1', d\bar{x}_2', d\bar{x}_3')$, $\bar{X} = (d\bar{x}_1, d\bar{x}_2, d\bar{x}_3)$, and $\mathcal{Q}$ and $\mathcal{Q}'$ are rotation matrices.

$$\mathcal{Q}' = \begin{bmatrix} \cos\alpha' & \sin\alpha' & 0 \\ -\sin\alpha' & \cos\alpha' & 0 \\ 0 & 0 & 1 \end{bmatrix}; \qquad \mathcal{Q} = \begin{bmatrix} \cos\alpha & \sin\alpha & 0 \\ -\sin\alpha & \cos\alpha & 0 \\ 0 & 0 & 1 \end{bmatrix} \tag{A7}$$

By putting *Eqs A3, A4,* and *A6* into *Eq A1*, one gets *Eq 8*:

$$C = \mathcal{Q} \cdot \{(\bar{X}^{-1})^T \cdot \bar{X}'^T \cdot \bar{X}' \cdot \bar{X}^{-1}\} \cdot \mathcal{Q}^{-1}. \tag{A8}$$

The velocity gradient tensor, ∇v, is given by

$$\nabla v = \begin{bmatrix} \dfrac{\partial v_t}{\partial x_t} & -\dfrac{v_t}{R} \\ \dfrac{\partial v_t}{\partial x_n} & \dfrac{\partial v_n}{\partial x_n} \end{bmatrix} \tag{A9}$$

where R is the radius of the curvature of the local coordinate system. The rate of change of a given material vector along a path line is related to the velocity gradient at the current point in the flow (25):

$$\frac{D}{Dt} dx = dx \cdot \nabla v \tag{A10}$$

where ∇v is the velocity gradient at t and $\dfrac{D}{Dt}$ is a material derivative. This ordinary differential equation is used for the purpose of tracking. *Equation A10* is general, but for steady incompressible planar flow, two pairs of vectors are calculated easily. The third pair needs only scalar integration. We assume the flow is steady and two-dimensional. By expanding *Eq A10*, applying the chain rule on *Eq A4*, and then setting the components of the resulting equations equal, one gets a pair of scalar equations:

$$\frac{da'}{dt'} = a' \frac{\partial v_t'}{\partial x_t'} - b' \frac{v_t'}{R'} + b' \frac{\partial v_t'}{\partial x_n'} \tag{A11}$$

$$\frac{db'}{dt'} = b' \frac{\partial v_n'}{\partial x_n'} \tag{A12}$$

These two equations may be combined, using the definition of γ in *Eq A4* to yield

$$\frac{d\gamma}{dt'} = \dot{\gamma}_{tn}' + 2\gamma \frac{\partial v_t'}{\partial x_t'} \tag{A13}$$

with

$$\dot{\gamma}_{tn} = \dot{\gamma} : x_n x_t = \frac{\partial v_t'}{\partial x_n'} - \frac{v_t'}{R'} \tag{A14}$$

Equation A13 can be written in integral form (*Eq A15*):

$$\left. \frac{\gamma''}{\rho'' v''^2} \right|_{t'}^{t} = \int_{t'}^{t} \frac{\dot{\gamma}_{tn}''}{\rho v''^2} \, dt''. \tag{A15}$$

When the term γ in *Eq A15* is chosen to be zero, it turns out to be identical with *Eq 19* by Winter (15).

ACKNOWLEDGMENT

We gratefully acknowledge the support of the Office of Naval Research under Contract N 00014-82-K-0083 and the support of General Electric Plastics, Pittsfield, Mass. Additionally, we thank the Digital Image Analysis Laboratory of the University of Massachusetts Computer Center for instruction and support. One of the authors, M. E. Nordberg III, acknowledges the additional support as a National Science Foundation Graduate Fellow.

NOMENCLATURE

a, b = tangent and normal components of material vector at time t.
a', b' = tangent and normal components of material vector at time t'.
C = stress-optical coefficient.
C_1, C_2 = material constants in WLF equation.
$\boldsymbol{C}$ = Cauchy-Green tensor.
$\boldsymbol{C}^{-1}$ = Finger strain tensor.
d = light path length.
E_0 = activation energy.
$\boldsymbol{F}$ = deformation gradient tensor.
f = material parameter in shear strain function.
g_i = discrete relaxation time coefficients.
h = strain functional.
I = generalized strain invariant, light intensity of emerging beam.
I_1, I_2 = first and second invariants of strain tensor respectively.
I_0 = light intensity of incident beam.
$\dot{m}$ = linear viscoelastic memory function.
m = memory function.
n = power-law exponent; refractive index.
$\boldsymbol{n}$ = unit normal vector on the stream surface.
n_1, n_2 = material parameters in shear strain function.
$\boldsymbol{Q}$ = rotation matrix.
R = radius of curvature of the streamline.
y_i = inner bound of the flow.
y_o = outer bund of the flow.
$\boldsymbol{t}$ = unit tangent vector on the stream surface.
T_0 = reference temperature.
v = magnitude of velocity vector.
v_t = velocity component along x_t-axis.
v_n = velocity component along x_n-axis.
x_1', x_2' = coordinates of initial position of material particle.
x_1 = distance from stagnation point along main flow direction.
x_2 = distance normal to x_1-axis coordinates.

Greek

α = material parameter in generalized strain invariant.
γ = shear strain.
γ' = tangent of shear angle.
$\dot{\gamma}$ = shear rate.
$\dot{\boldsymbol{\gamma}}$ = rate of deformation tensor.
δ = phase angle.
η_0 = zero shear rate viscosity.
η_∞ = infinite shear rate viscosity.
λ = time constant in Carreau model.
λ_i = discrete relaxation times.
ρ = density.
$\boldsymbol{\tau}$ = extra stress tensor.
ψ = streamlines of planar flow.

REFERENCES

1. H. H. Winter and K. H. Wei, "Interrelations between Processing and Properties of Polymeric Materials," J. C. Seferis and P. S. Theocaris, eds., Elsevier, Amsterdam, p. 261 (1984).
2. H. Janeschitz-Kriegl, "Polymer Melt Rheology and Flow Birefringence," Springer-Verlag, Berlin Heidelberg (1983).
3. T. Matsumoto and D. C. Bogue, *J. Polym. Sci., Polym. Phys. Ed.*, 15, 1663 (1977).
4. J. A. Van Aken, F. H. Gortemaker, H. Janeschitz-Kriegl, and H. M. Laun, *Rheol. Acta.*, 19, 159 (1980).
5. R. D. Pike and D. G. Baird, *J. Non-Newt. Fluid Mech.*, 16, 211 (1984).
6. A. I. Isayev and R. K. Upadhyay, *J. Non-Newt. Fluid Mech.*, 19, 135 (1985).
7. R. B. Bird, R. C. Armstrong, and O. Hassager, "Dynamics of Polymeric Liquids," Vol. 1, John Wiley (1977).
8. A. S. Lodge, R. C. Armstrong, M. H. Wagner, and H. H. Winter, *Pure Appl. Chem.*, 54, 1349 (1982).
9. A. S. Lodge, *Rheol. Acta*, 1, 158 (1958).
10. D. O. Doughty and D. C. Bogue, *Ind. Eng. Chem. Fundam.* 6, 388 (1967).
11. K. Osaki, Proc. VIIIth Int. Congr. Rheol., p. 104 Gothenburg (1976)
12. H. M. Laun, *J. Rheology*, 30, 459 (1986).
13. A. Demarmels and J. Meissner, *Colloid Polym. Sci.*, 264, 829 (1986).
14. M. J. Crochet, A. R. Davies, and K. Walters, "Numerical Simulation of Non-Newtonian Flow," Elsevier, Amsterdam (1984).
15. H. H. Winter, *J. Non-Newt. Fluid Mech.*, 10, 157 (1982).
16. J. V. Lawler, S. J. Muller, R. A. Brown, R. C. Armstrong, *J. Non. Newt. Fl. Mech.* 20, 51 (1986).
17. K. H. Wei, M. F. Malone, and H. H. Winter, *Polym. Eng. Sci.*, 26, 1012 (1986).
18. M. Viriyayuthakorn and B. Caswell, *J. Non-Newt. Fluid Mech.*, 8, 245 (1981).
19. B. Bernstein, M. K. Kadivar, and D. S. Malkus, *Comp. Meth. Appl. Mech. Eng.*, 27, 279 (1981).
20. S. Dupont, J. M. Marchal, and M. J. Crochet, *J. Non-Newt. Fluid Mech.*, 17, 157 (1985).
21. K. Adachi, *Rheol. Acta* 25, 555 (1986).
22. M. E. Nordberg III, Ph.D. Thesis, University of Massachusetts (in progress).
23. J. L. S. Wales, Ph.D. Thesis, Delft University (1976).
24. P. R. Soskey and H. H. Winter, *J. Rheology*, 28, 625 (1984).
25. C. Truesdell, "A First Course in Rational Continuum Mechanics," Vol. 1, Academic Press, New York (1977).